

Efficient construction of involutory linear combinations of anti-commuting Pauli generators for large-scale iterative qubit coupled cluster calculations

Ilya G. Ryabinkin,^{*,†} Andrew J. Jena,[‡] and Scott N. Genin[†]

[†]*OTI Lumionics Inc., 3415 American Drive Unit 1,
Mississauga, Ontario L4V 1T4, Canada*

[‡]*Combinatorics & Optimization, University of Waterloo
Waterloo, Ontario, N2L 3G1, Canada*

E-mail: ilya.ryabinkin@otilumionics.com

January 26, 2023

Abstract

We present an efficient method for construction of a fully anti-commutative set of Pauli generators (elements of the Pauli group) from a commutative set of operators that are composed exclusively from Pauli \hat{x}_i operators (purely X generators) and sorted by an associated numerical measure, such as absolute energy gradients. Our approach uses the Gauss–Jordan elimination applied to a binary matrix that encodes the set of X generators to bring it to the reduced row echelon form, followed by the construction of an anti-commutative system in a standard basis by means of a modified Jordan-Wigner transformation and returning to the original basis. The algorithm complexity is linear

in the size of the X set and quadratic in the number of qubits. The resulting anti-commutative sets are used to construct the qubit coupled cluster Ansatz with involutory linear combinations of anti-commuting Paulis (QCC-ILCAP) proposed in [J. Chem. Theory Comput. **2021**, *17*, 1, 66–78]. We applied the iterative qubit coupled cluster method with the QCC-ILCAP Ansatz to calculations of ground-state potential energy curves for symmetric stretching of the water molecule (36 qubits) and dissociation of N_2 (56 qubits).

1 Introduction

Quantum chemistry calculations are among the most promising applications of quantum computing. A lot of efforts have been spent towards quantum computer-friendly algorithms for solving the electronic structure problem in particular.^{1–5} The major obstacle in designing such algorithms is that the current and near-term quantum computers are the noisy intermediate-scale quantum (NISQ)⁶ devices featuring limited number of qubits, limited connectivity, short coherence times and high levels of noise. To cope with these limitations, the variational quantum eigensolver (VQE) approach has been proposed.⁷ In VQE-based methods a quantum computer runs a parametrized quantum circuit to prepare a trial quantum state, then Hamiltonian terms are repeatedly measured individually or in groups^{8–13} on this state to obtain the ground-state energy estimate. Subsequently, accumulated estimates are used by a classical computer to predict a location of the energy minimum via gradient-free optimization; updated parameters are returned back to a quantum computer thus forming a quantum-classical feedback loop. Recently, efficient algorithms for measuring energy gradients on a quantum computer have also been proposed^{14,15} allowing for the use of gradient-based minimization schemes.¹⁶

The quantum circuit represents a unitary transformation $\hat{U}(\mathbf{t})$ of a reference state $|0\rangle$ into

a target state $|\Psi(\mathbf{t})\rangle$ for a set of user-controlled parameters $\mathbf{t} = t_1, \dots, t_L$:

$$|\Psi(\mathbf{t})\rangle = \hat{U}(\mathbf{t}) |0\rangle. \quad (1)$$

The unitary transformation must be realizable on a quantum computer – in other words, it must be readily translated into a sequence of quantum gates without additional approximations. This can be trivially achieved if $\hat{U}(\mathbf{t})$ is directly encoded in terms of gates available on particular quantum hardware¹⁷ but a far more popular approach is to employ some universal, hardware-independent intermediate representation. As such, a product of exponents of Pauli generators \hat{T}_k is used:

$$\hat{U}(\mathbf{t}) = \prod_{k=1}^L \exp\left(-it_k \hat{T}_k / 2\right). \quad (2)$$

Generators (“Pauli words”)

$$\hat{T}_k = \prod_{j \geq 0, j \in j(k)} \hat{\sigma}_j, \quad (3)$$

are strings (tensor products) of Pauli elementary operators $\hat{\sigma}_j = \hat{x}_j, \hat{y}_j, \text{ or } \hat{z}_j$, where $0 \leq j \leq (n - 1)$ and n is the number of qubits. There are $4^n - 1$ non-trivial Pauli words for n qubits; together with the identity operator $\hat{\mathcal{I}}$ and phase factors $\pm 1, \pm i$ they constitute 4^{n+1} -element Pauli group with respect to multiplication.¹⁹

Equation (2) is the final form for many VQE-based methods.^{7,20–29} They differ, however, in the way how generators \hat{T}_k are selected and ordered. The qubit coupled cluster (QCC) method²⁵ constructs the Ansatz (2) directly by selecting appropriate elements of Pauli group based on the energy gradient criterion. As we have shown,²⁹ there exists a linearly scaling (in the number of Hamiltonian terms) algorithm that allows one to rank Pauli words in their projected importance for the energy lowering. Paired with the iterative approach, this ranking scheme constitutes a basis for the iterative qubit coupled cluster (iQCC) method, which has been subsequently augmented with perturbative completeness corrections to treat large (more than 70 qubits) systems.^{30,31}

Besides suitability for quantum computers, Eq. (2) is straightforward to implement on classical computers. Because Pauli words with unit phases are involutory operators,

$$\hat{T}_k^2 = \hat{\mathcal{I}}, \quad \forall k, \quad (4)$$

their exponentiation is trivial:

$$\exp\left(-\frac{it_k\hat{T}_k}{2}\right) = \cos\left(\frac{t_k}{2}\right) - i \sin\left(\frac{t_k}{2}\right) \hat{T}_k. \quad (5)$$

Plugging Eq. (5) into Eq. (2) and expanding, we obtain a sum of 2^L terms

$$\hat{U}(\mathbf{t}) = \prod_{k=1}^L \cos\left(\frac{t_k}{2}\right) - i \sum_{j=1}^L \hat{T}_j \sin\left(\frac{t_j}{2}\right) \prod_{k \neq j}^L \cos\left(\frac{t_k}{2}\right) - \dots \quad (6)$$

thus illustrating the exponential complexity of the Ansatz. While this complexity is not a problem for a perfect quantum computer—and can be even considered as quantum advantage—it is an obstacle for classical simulators and for implementation of various pre- and post-processing techniques that decrease the amount of work performed by a NISQ device.

An Ansatz that is characterized by linear, not exponential, complexity has been proposed in Ref. 32. It is based on a few simple ideas. The closed form of the exponent of generators, Eq. (5) exists because of the involutory property of Pauli words, Eq. (4). Hence, one can try to generalize this property to linear combinations of Pauli words, namely, if

$$\hat{T} = \sum_{k=1}^M \alpha_k \hat{T}_k, \quad (7)$$

$$\hat{T}^2 = \hat{\mathcal{I}}, \quad (8)$$

then

$$\begin{aligned}\hat{U}(t, \boldsymbol{\alpha}) &= \exp\left(-\frac{it\hat{T}}{2}\right) = \cos\left(\frac{t}{2}\right) - i \sin\left(\frac{t}{2}\right) \hat{T} \\ &= \cos\left(\frac{t}{2}\right) - i \sin\left(\frac{t}{2}\right) \sum_{k=1}^M \alpha_k \hat{T}_k.\end{aligned}\tag{9}$$

Performing elementary algebraic manipulations with Eqs. (7) and (8) we obtain:

$$\sum_{k=1}^M \alpha_k^2 = 1,\tag{10}$$

$$\left[\hat{T}_k, \hat{T}_m\right]_+ = 0, \quad 1 \leq k, m \leq M, \quad k \neq m\tag{11}$$

where $[\hat{A}, \hat{B}]_+ = \hat{A}\hat{B} + \hat{B}\hat{A}$ is the anti-commutator. Thus, the vector of coefficients $\boldsymbol{\alpha}$ must be normalized, and Pauli words must be all anti-commuting. In general, any two Pauli words are either commuting or anti-commuting, hence, there exist some non-trivial (i.e. with $M \geq 2$) linear combinations of Paulis that satisfy Eq. (11). The main result of Ref. 32 is that $M \leq 2n - 1$ where n is the number of qubits when \hat{T}_k are subjected to the gradient condition, which *guarantees* the energy lowering in VQE optimization to avoid the so-called *barren plateaus*.³³ Reference 32 has also presented a proof-of-the-principle algorithm for constructing such involutory linear combinations of anti-commuting Paulis (ILCAP).

The current paper builds upon and extends Ref. 32. First of all, we propose a new algorithm for constructing the anti-commuting sets of Pauli operators from a set of those that are “tagged” by an additional property, such as the absolute energy gradient (see Sec. 2.1). Our algorithm makes use of Gauss–Jordan elimination for matrices with coefficients from the Galois field GF(2) – the binary numbers 0 and 1. It is highly efficient and allows for dealing with problems with the number of qubits $n \gtrsim 100$ and Hamiltonians containing billions of terms. Contrary to the original algorithm from Ref. 32 it does not require any trial-and-error steps. Finally, the new algorithm is capable of attaining the upper limit for the size of anti-commuting sets, $M = 2n - 1$ though practical considerations may suggest

lower M .

The paper is organized as follows. First, we briefly outline the iQCC method. Secondly, we introduce a new algorithm for constructing systems of anti-commuting generators. Then we discuss a new variant of the perturbation-theory correction to the QCC-ILCAP Ansatz and compare it to the perturbative correction proposed in Ref. 30. Finally, we assess the performance of the QCC-ILCAP Ansatz as a pre- and post-processing technique within the “standard” iQCC method on cases of large-scale CI calculations for symmetric dissociation of the H₂O molecule and stretching of the N₂ molecule.

2 Theory

2.1 An outline of the iQCC method

The iQCC method takes an active-space second-quantized electronic Hamiltonian of a molecule,^{7,34–36}

$$\hat{H}_e = E_{\text{core}} + \sum_{ij} f_{ij} \hat{a}_i^\dagger \hat{a}_j + \frac{1}{2} \sum_{ijkl} g_{ijkl} \hat{a}_i^\dagger \hat{a}_j^\dagger \hat{a}_l \hat{a}_k, \quad (12)$$

as input. \hat{a}_i^\dagger and \hat{a}_i are fermion creation and annihilation operators in the active space, E_{core} is the electronic energy associated with inactive (core) orbitals, f_{ij} , and g_{ijkl} are one- and two-electron contributions to the electronic energy written in a spin-orbital basis.

$$g_{ijkl} = \iint \frac{\psi_i^*(\mathbf{x}_1) \psi_k^*(\mathbf{x}_2) \psi_j(\mathbf{x}_1) \psi_l(\mathbf{x}_2)}{r_{12}} d\mathbf{x}_1 d\mathbf{x}_2 \quad (13)$$

where $\mathbf{x} = (\mathbf{r}, \sigma)$. f_{ij} account for the kinetic and nuclear-attraction energy of active electrons as well as their electrostatic interaction with core electrons.

Prior to any computations, the Hamiltonian (12) is converted to a qubit form by the

Jordan–Wigner (JW) transformation^{36,37} to obtain

$$\hat{H} = \sum_{k=1}^M C_k \hat{P}_k, \quad (14)$$

where C_k are coefficients inferred from f_{ij} and g_{ijkl} and \hat{P}_k are Pauli words.

Apart from the Hamiltonian, the iQCC method requires a reference vector $|0\rangle$ to be specified. As such, a direct-product state,

$$|0\rangle = \prod_{k=1}^{n_e} |\downarrow\rangle_k \times \prod_{k=1}^{n-n_e} |\uparrow\rangle_k \quad (15)$$

is used. Here n_e is the number of electrons in the active space for an electronic state of interest and n is the total number of qubits which is equal to the number of active spin-orbitals. If n is twice the size of an atomic basis and n_e equals to the total number of electrons in a molecule (hence, $E_{\text{core}} = 0$), one deals with the full configurational interaction (FCI) problem, otherwise it is a complete active space configurational interaction (CASCI) problem with an active space which is commonly abbreviated as CAS($n_e, n/2$). $|\uparrow\rangle_k$ and $|\downarrow\rangle_k$ are eigenstates of \hat{z}_k with eigenvalues $+1$ and -1 , respectively. We additionally assume pairwise grouping of spin-orbitals: the first orbital with α (“up”) spin is mapped to the first qubit, followed by the first orbital with β spin, which is mapped to the second, etc. There is one-to-one correspondence between spin-orbital population strings for fermions and product states of qubits if the JW transformation is employed. Thus, if the basis of Hartree–Fock molecular orbitals (MOs) is used, $|0\rangle$ represents an electron configuration that satisfies the Aufbau principle, which is typically the lowest-energy configuration.

An essential feature of the iQCC method is how generators \hat{T}_k are selected and ordered (“ranked”) to be used in the Ansatz (2). For the sake of brevity we introduce the simplest gradient-based ranking scheme; other possibilities are discussed in Ref. 30. Consider a single-generator QCC Ansatz, $\hat{U}(t) = \exp(-it\hat{T}/2)$, and compute the energy expectation

value for $|\Psi(t)\rangle = \hat{U}(t)|0\rangle$:

$$E[\hat{T}](t) = \langle \Psi(t) | \hat{H} | \Psi(t) \rangle = \langle 0 | \exp(it\hat{T}/2) \hat{H} \exp(-it\hat{T}/2) | 0 \rangle. \quad (16)$$

Using Eq. (5) one can further elaborate the expression for $E[\hat{T}](t)$:

$$E[\hat{T}](t) = \langle 0 | \hat{H} | 0 \rangle + \frac{\sin(t)}{2i} \langle 0 | [\hat{H}, \hat{T}] | 0 \rangle + \frac{1 - \cos(t)}{2} \langle 0 | (\hat{T} \hat{H} \hat{T} - \hat{H}) | 0 \rangle, \quad (17)$$

where $[\hat{A}, \hat{B}] = \hat{A}\hat{B} - \hat{B}\hat{A}$ is a commutator. Defining

$$\omega = \left| \frac{1}{2i} \langle 0 | [\hat{H}, \hat{T}] | 0 \rangle \right| = \left| \Im \langle 0 | \hat{H} \hat{T} | 0 \rangle \right|, \quad (18)$$

we notice that ω is an absolute value of the energy gradient at $t = 0$. Generators with non-zero ω *guarantee* the energy lowering being used in the QCC Ansatz (2). Thus, one can use ω for sorting generators taking \hat{T}_k with larger ω_k first.

All generators with a priori non-zero values of ω can be efficiently constructed given the Ising decomposition of the Hamiltonian,^{29,30} which reads

$$\hat{H} = \hat{I}_0(\mathbf{z}) + \sum_{k>0} \hat{I}_k(\mathbf{z}) \hat{X}_k, \quad (19)$$

where $\hat{I}_k(\mathbf{z})$, $k = 0, 1, \dots$ are qubit Hamiltonians that are sums of Pauli words containing only Pauli elementary \hat{z} operators (“generalized Ising Hamiltonians”). All \hat{X}_k are the Pauli X strings,

$$\hat{X}_k = \prod_{j \geq 0, j \in j(k)} \hat{x}_j. \quad (20)$$

The decomposition (19) does not contain Pauli \hat{y} operators because they are factorized as $\hat{y}_j = -i\hat{z}_j\hat{x}_j$.

As was shown in Ref. 29, there are 2^{n-1} generators \hat{T}_{k_i} for every *single* \hat{X}_k that appears in the decomposition (19), which are all characterized by the same value of the absolute energy

gradient determined solely by the parental \hat{X}_k :

$$\omega_k = \left| \langle 0 | \hat{I}_k | 0 \rangle \right|. \quad (21)$$

They all can be obtained from \hat{X}_k by substituting an *odd* number of elementary \hat{x}_j operators with their \hat{y}_j counterparts and adding an arbitrary number of \hat{z} operators with qubit indices that are *not* in \hat{X}_k . This redundancy is exploited in the original iQCC method to define a “canonical set” of generators: \hat{T}_k are created by converting a *single* \hat{x}_j with the smallest possible j in every \hat{X}_k into \hat{y}_j . More importantly, it provides necessary flexibility for finding $M \geq 2$ anti-commuting generators satisfying Eq. (11).

After ranking and selecting generators at the i -th iteration, the iQCC method minimizes the QCC energy expression

$$E^{(i)}(t_1, \dots, t_L) = \left\langle 0 \left| \left(\hat{U}^{(i)} \right)^\dagger (t_1, \dots, t_L) \hat{H}^{(i)} \hat{U}^{(i)}(t_1, \dots, t_L) \right| 0 \right\rangle, \quad i = 1, \dots \quad (22)$$

where $\hat{H}^{(i)}$ is the current Hamiltonian [$\hat{H}^{(1)} = \hat{H}$ is the original electronic Hamiltonian in qubit representation, Eq. (14)], and $\hat{U}^{(i)}$ is the QCC Ansatz (2) with L topmost generators constructed using the Ising decomposition of $\hat{H}^{(i)}$.

Once the energy is minimized, the iQCC algorithm performs *dressing* of the current Hamiltonian $\hat{H}^{(i)}$. Dressing is a unitary transformation of $\hat{H}^{(i)}$ using $\hat{U}^{(i)}(\mathbf{t}_{\text{opt}}^{(i)})$ where $\mathbf{t}_{\text{opt}}^{(i)}$ are the optimized amplitudes. Below we demonstrate the first step of this transformation, which corresponds to $L = 1$ in Eq. (2); subsequent steps (for $L > 1$) are performed recursively:

$$\hat{H}^{(i+1)} = \left(\hat{U}^{(i)} \right)^\dagger (t_{1,\text{opt}}^{(i)}) \hat{H}^{(i)} \hat{U}^{(i)}(t_{1,\text{opt}}^{(i)}) \quad (23)$$

$$= \hat{H}^{(i)} - \frac{i}{2} \sin \left(t_{1,\text{opt}}^{(i)} \right) [\hat{H}^{(i)}, \hat{T}_1] + \frac{1 - \cos(t_{1,\text{opt}}^{(i)})}{2} \left(\hat{T}_1 \hat{H}^{(i)} \hat{T}_1 - \hat{H}^{(i)} \right). \quad (24)$$

If dressing is performed exactly (i.e. without rounding), the following identity is hold:

$$\langle 0 | \hat{H}^{(i+1)} | 0 \rangle = E^{(i)}(t_{1,\text{opt}}^{(i)}, \dots, t_{L,\text{opt}}^{(i)}). \quad (25)$$

The identity (25) allows one to complete an iQCC loop. One can start a new iteration taking $\hat{H}^{(i+1)}$ as an initial Hamiltonian while keeping the reference vector $|0\rangle$ intact. The iterative procedure then proceeds until some convergence criteria (e.g. largest ω is less than a threshold) are met. The QCC energy at the final iteration then becomes the ground-state energy estimate. We emphasise that, contrary to the VQE-style methods based on the unitary coupled cluster (UCC) hierarchy with limited excitation rank (e.g. UCCSD), the iQCC method is *exact*, in other words, it is capable of attaining the CASCI or FCI energy of a system.

2.2 Constructing a set of mutually anti-commuting generators

2.2.1 A problem statement

Given a set of Pauli X words $\hat{X}_1, \hat{X}_2, \dots, \hat{X}_m \equiv \{\hat{X}_m\}$ that are taken from the Ising decomposition (19) of the current Hamiltonian and ordered according to their absolute gradients $\omega_1 \geq \omega_2 \geq \dots \geq \omega_m$, Eq. (21), find a largest subset $\{\hat{X}_{m_l}\} \subseteq \{\hat{X}_m\}$, and construct a set of complementary Z words $\{\hat{Z}_{m_l}\}$, such that the “phaseless” products $\hat{T}_{m_l} = \hat{X}_{m_l} \odot \hat{Z}_{m_l}$ contain the *odd* number of Pauli elementary operators \hat{y} and satisfy Eq. (11). The phaseless multiplication follows the normal multiplication rule for the Pauli elementary operators but ignores the resulting phases $\pm i$ completely, that is, for example, $\hat{x} \odot \hat{y} = \hat{y} \odot \hat{x} = \hat{z}$. The condition on the odd number of \hat{y} factors in every \hat{T}_{m_l} ensures that the real part of the energy gradient $dE[\hat{T}_{m_l}]/dt \Big|_{t=0}$ is non-zero.

2.2.2 An outline of the solution

The solution is found in a few steps. First, we employ the binary encoding³⁸ to map Pauli words to column vectors of the length n with 0 and 1 as entries. Consequently, the set

$\{\hat{X}_m\}$ can be represented as a $n \times m$ matrix \mathbf{M} whose columns are the binary vectors X_1, X_2 , etc. Second, we show that two universal qubit transformations, namely, CNOT and SWAP gates, in the binary representation become the elementary matrix transformations of \mathbf{M} , row-addition and row-switching, respectively. This correspondence allows us to apply Gauss–Jordan elimination to \mathbf{M} to bring it to the reduced row-echelon form,⁴⁰ \mathbf{M}_{ref} . The columns of \mathbf{M}_{ref} containing the leading 1 are identified with a subset of all Pauli elementary operators $\{\hat{x}_j\}_{j=0}^{(n-1)}$. Then we show how to convert elementary Pauli x operators into $(2n - 1)$ *anti-commuting* operators with the odd number of \hat{y} factors using a slightly modified Jordan–Wigner transformation. Speaking informally, the JW-construction solves our problem by finding such Pauli Z words that make the “standard” basis of \hat{x}_j anti-commutative. Finally, we map a binary representation of those Z words back to the original basis to determine $\{\hat{Z}_{m_i}\}$ which completes our algorithm.

2.2.3 Binary encodings for X and Z Pauli words and a matrix M

Let us assume that the number of qubits n is fixed. Then, any Pauli X word can be mapped into an n -dimensional column vector $(\dots 1 \dots 0 \dots)^T$ by setting 1 in the position i as long as \hat{x}_{i-1} enters the word. For example, the word $\hat{X} = \hat{x}_0\hat{x}_2$ for $n = 4$ is mapped to $(1010)^T$. Similarly, any Z word can be mapped into an n -vector by applying the same rule. A *general* Pauli word \hat{P} , thus, can be represented as $2n$ -dimensional vector $(X|Z)^T$ according to the factorization $\hat{P} = \hat{X} \odot \hat{Z}$.³⁸ Since we will be always dealing with factorized expressions, it is sufficient to consider the n -dimensional binary representations for X and Z words separately.

Consider a sequence of Pauli words $\{\hat{X}_m\} = \hat{X}_1, \hat{X}_2, \dots$ that are taken from the Ising decomposition (19) and arranged according to their absolute gradients $\omega_1 \geq \omega_2 \geq \dots$. The corresponding binary vectors X_1, X_2, \dots are the columns of a matrix \mathbf{M} . For example, a 5-element sequence of X words

$$\{\hat{x}_0\hat{x}_2, \hat{x}_1\hat{x}_3, \hat{x}_0\hat{x}_1\hat{x}_2, \hat{x}_1\hat{x}_2\hat{x}_3, \hat{x}_0\hat{x}_1\hat{x}_2\hat{x}_3\} \quad (26)$$

for $n = 4$ qubits is encoded as a 4×5 matrix

$$\begin{pmatrix} 1 & 0 & 1 & 0 & 1 \\ 0 & 1 & 1 & 1 & 1 \\ 1 & 0 & 1 & 1 & 1 \\ 0 & 1 & 0 & 1 & 1 \end{pmatrix}. \quad (27)$$

2.2.4 CNOT and SWAP quantum gates and Gauss–Jordan elimination

CNOT and SWAP quantum gates acts on elements of the Pauli group by conjugation, $\hat{P} \rightarrow \hat{U}\hat{P}\hat{U}^\dagger$, where \hat{P} is an arbitrary element and $\hat{U} \in \{\text{CNOT}, \text{SWAP}\}$. Their action is summarized in Table 1.

Table 1: Transformation properties of elements of the Pauli group under conjugation by CNOT and SWAP gates.⁴² CNOT₁₂ has qubit 1 as the control and qubit 2 as the target, SWAP₁₂ acts on qubits 1 and 2.

Operation	Input	Output
CNOT	\hat{x}_1	$\hat{x}_1\hat{x}_2$
	\hat{x}_2	\hat{x}_2
	\hat{z}_1	\hat{z}_1
	\hat{z}_2	$\hat{z}_1\hat{z}_2$
SWAP	\hat{x}_1	\hat{x}_2
	\hat{z}_1	\hat{z}_2

It must be noted that the SWAP gate can be implemented as a sequence of CNOT gates; for our purposes, however, it is convenient to define SWAP as an independent operation to make a perfect connection with the elementary matrix transformations (see below). We also note that both gates are unitary and self-inverse, for example, $\text{CNOT} = \text{CNOT}^\dagger = \text{CNOT}^{-1}$, so that in Table 1 inputs and outputs can be exchanged.

It is clear from Table 1 that conjugation of all operators from $\{\hat{X}_m\}$ with CNOT₁₂ – here we explicitly show what are the control and target qubits of the CNOT operation – is equivalent

to adding the first row of the matrix \mathbf{M} [cf. Eq. (27)] to its second row modulo 2. Similarly, conjugation with SWAP_{12} is a transposition of rows 1 and 2. By using CNOT_{ij} or SWAP_{ij} we extend these operations to arbitrary qubits i and j and the corresponding rows of \mathbf{M} . That is, we established a connection between certain transformations of Pauli words and elementary matrix operations that are used in the Gauss–Jordan elimination procedure. The latter applied to a matrix \mathbf{M} allows one to bring it to the reduced row-echelon form. Again, considering the example of the 4×5 matrix \mathbf{M} , Eq. (27), we obtain:

$$\mathbf{M}_{\text{ref}} = \begin{pmatrix} 1 & 0 & 0 & 0 & 1 \\ 0 & 1 & 0 & 0 & 1 \\ 0 & 0 & 1 & 0 & 0 \\ 0 & 0 & 0 & 1 & 0 \end{pmatrix}. \quad (28)$$

We shall call columns of \mathbf{M}_{ref} with the leading 1 [e.g. columns 1–4 in Eq. (28)] the *primary* columns (vectors). These columns correspond to the Pauli elementary operators \hat{x}_i in the binary representation.

A matrix \mathbf{R} that brings \mathbf{M} to its reduced row echelon form, $\mathbf{RM} = \mathbf{M}_{\text{ref}}$, can be found by applying Gauss–Jordan elimination to an augmented matrix $(\mathbf{M}|\mathbf{E})$, where \mathbf{E} is the $n \times n$ identity matrix. After the full execution of Gauss–Jordan elimination it becomes $(\mathbf{M}_{\text{ref}}|\mathbf{R})$.

2.2.5 $(2n - 1)$ anti-commuting operators from a modified JW transformation

By means of Gauss–Jordan elimination we mapped certain Pauli X words from $\{\hat{X}_m\}$ to the Pauli elementary operators \hat{x}_i . We are now in a position to demonstrate how to convert them into a set anti-commuting Pauli words with the odd number of \hat{y} co-factors. To this end let us recall the standard Jordan–Wigner construction, which maps qubit (spin) operators \hat{x}_i

and \hat{y}_i into anti-commuting Majorana operators ^a

$$\hat{x}_i \rightarrow \hat{C}_i = \hat{x}_i \prod_{j=0}^{i-1} \hat{z}_j, \quad (29)$$

$$\hat{y}_i \rightarrow \hat{D}_i = \hat{y}_i \prod_{j=0}^{i-1} \hat{z}_j = i \hat{x}_i \prod_{j=0}^i \hat{z}_j, \quad (30)$$

where $0 \leq i \leq (n-1)$. There are $2n$ fully anti-commutative operators $\{\hat{C}_i\}_{i=0}^{n-1}$ and $\{\hat{D}_i\}_{i=0}^{n-1}$. The $(2n+1)$ -th anti-commuting operator $\hat{\Xi}$ is a product of all \hat{C}_i and \hat{D}_i ; it is equal to

$$\hat{\Xi} = \prod_{j=0}^{n-1} \hat{z}_j. \quad (31)$$

Operators $\{\hat{D}_i\}_{i=0}^{n-1}$ already have the odd number of \hat{y} co-factors. The remaining $(n+1)$ operators have no \hat{y} at all. However, it is possible to define $(n-1)$ operators with an odd number of \hat{y} as

$$\hat{F}_i = i \hat{C}_0 \hat{C}_i \hat{\Xi} = i \hat{x}_0 \hat{x}_i \prod_{j=i}^{n-1} \hat{z}_j = \hat{x}_0 \hat{y}_i \prod_{j=i+1}^{n-1} \hat{z}_j, \quad 1 \leq i \leq (n-1) \quad (32)$$

Direct calculations using the full anti-commutativity of \hat{C}_i , \hat{D}_i , and $\hat{\Xi}$ show that $[\hat{F}_i, \hat{F}_j]_+ = 0$ for $i \neq j$ and $[\hat{D}_i, \hat{F}_j]_+ = 0$. Thus, we have constructed a set of $(2n-1)$ fully anti-commutative operators $\{\hat{D}_i\}_{i=0}^{(n-1)}$ and $\{\hat{F}_i\}_{i=1}^{(n-1)}$ which all have the odd number of \hat{y} co-factors.

^aMajorana fermion operators \hat{C}_i and \hat{D}_i , are related to the ordinary (Dirac) fermion creation and annihilation operators as

$$\begin{aligned} \hat{a}_i &= \frac{1}{2} (\hat{C}_i + i \hat{D}_i), \\ \hat{a}_i^\dagger &= \frac{1}{2} (\hat{C}_i - i \hat{D}_i). \end{aligned}$$

2.2.6 A set of anti-commuting operators from $\{\hat{X}_m\}$

Eqs. (30) and (32) demonstrate how to convert Pauli words $\{\hat{x}_i\}_{j=0}^{(n-1)}$ and $\{\hat{x}_0\hat{x}_i\}_{j=1}^{(n-1)}$ into a $(2n-1)$ -member set of fully anti-commutative operators by appending Z words $\left\{\prod_{j=0}^i \hat{z}_j\right\}_{i=0}^{n-1}$ and $\left\{\prod_{j=i}^{n-1} \hat{z}_j\right\}_{i=1}^{n-1}$, respectively. These operators are defined in the representation in which the matrix \mathbf{M} is brought to the reduced row-echelon form. The primary columns of the matrix \mathbf{M}_{ref} correspond to a subset of $\{\hat{x}_i\}_{j=0}^{(n-1)}$. In turn, columns of \mathbf{M}_{ref} that have the binary representation $(\mathbf{1}0 \dots 0\mathbf{1}_i0 \dots 0)^T$ are associated with a subset of $\{\hat{x}_0\hat{x}_i\}_{j=1}^{(n-1)}$; we shall refer to such vectors as “secondary”. In the example (28) the last column represents a single secondary vector.

Primary and secondary Z operators (and corresponding vectors) are defined as partners of primary/secondary X operators in Eqs. (30) and (32). We collect all definitions in Table 2.

Table 2: Primary and secondary X and Z operators whose products $\hat{T}_k = \hat{X}_k \odot \hat{Z}_k$ are fully anti-commutative. The total length of the strings in the binary representation is n , which is the number of qubits.

Type	Classification	Operator form	Binary representation
X words	Primary	\hat{x}_i	$(0 \dots 0\mathbf{1}_i0 \dots 0)^T$
	Secondary	$\hat{x}_0\hat{x}_i$	$(\mathbf{1}0 \dots 0\mathbf{1}_i0 \dots 0)^T$
Z words	Primary	$\prod_{j=0}^i \hat{z}_j$	$(\mathbf{1} \dots \mathbf{1}_i0 \dots 0)^T$
	Secondary	$\prod_{j=i}^{(n-1)} \hat{z}_j$	$(0 \dots 0\mathbf{1}_i \dots \mathbf{1})^T$

It is important to emphasize that *only primary and secondary vectors of \mathbf{M}_{ref} can be used to create the anti-commutative system*. The number of such vectors is uniquely determined by \mathbf{M} and, in turn, by the composition and ordering of $\{\hat{X}_m\}$.

Our final task is to return to the original basis. For X words this operation is trivial: the inverse transform \mathbf{R}^{-1} brings the primary and secondary columns of \mathbf{M}_{ref} back to the corresponding columns of \mathbf{M} . These columns hence determine a subset $\{\hat{X}_{m_i}\}$ of Pauli words in $\{\hat{X}_m\}$ that participate in formation of the anti-commutative system. The solution is slightly more involved for Z words. A careful inspection of Table 1 shows that the CNOT

operation acts on Z words as a *transposed* row-addition elementary operation. We have to also reverse the ordering of operations in the Gauss–Jordan elimination, so that if $\mathbf{R} = \mathbf{R}_1 \cdots \mathbf{R}_k$ then the desired transformation is $(\mathbf{R}_k^{-1})^T \cdots (\mathbf{R}_1^{-1})^T$ and since $\mathbf{R}_j^{-1} = \mathbf{R}_j$ (modulo 2), it is equivalent to $\mathbf{R}_k^T \cdots \mathbf{R}_1^T = \mathbf{R}^T$. Thus, one has to apply \mathbf{R}^T to the primary and secondary binary Z vectors (see rows 4–5 of Table 2) to generate the corresponding Z vectors in the original representation and, subsequently, to recover Z words that are partners of X words in $\{\hat{X}_{m_i}\}$. The resulting operators $\hat{T}_{m_i} = \hat{X}_{m_i} \odot \hat{Z}_{m_i}$ are all mutually anti-commutative, $[\hat{T}_{k'}, \hat{T}_k]_+ = 0$ for $k' \neq k$, because anti-commutativity is preserved by conjugation with CNOT and SWAP gates. Completing the example given by Eqs. (26), (27), and (28), we find the following anti-commuting system:

$$\{\hat{y}_0 \hat{z}_1 \hat{x}_2 \hat{z}_3, \hat{y}_1 \hat{z}_2 \hat{x}_3, \hat{x}_0 \hat{x}_1 \hat{y}_2 \hat{z}_3, \hat{z}_0 \hat{x}_1 \hat{x}_2 \hat{y}_3, \hat{x}_0 \hat{y}_1 \hat{x}_2 \hat{x}_3\}. \quad (33)$$

Every \hat{T}_{m_i} contains the odd number of \hat{y} factors, albeit not necessarily a *single* such factor like operators in the standard system $\{\hat{D}_i\} \cup \{\hat{F}_i\}$ [see Eqs. (30) and (32)]. This remarkable fact can be proven as follows. Pauli words with the odd number of \hat{y} factors are *imaginary* operators – their matrices have purely imaginary elements in the tensor-product basis of eigenstates of \hat{z}_i , $0 \leq i \leq (n - 1)$. CNOT and SWAP gates are purely real matrices in the same basis, so that the imaginary matrices (hence, operators) in the standard basis remains imaginary under conjugation with any of these operators.

2.2.7 Practical considerations

There is still a great deal of flexibility in the algorithm. The resulting set of anti-commuting Paulis depends on the ordering of columns of the matrix \mathbf{M} and hence, the ordering of operators in $\{\hat{X}_m\}$. We always take an operator with the largest gradient (or another “importance measure”, see Ref. 30) as first, which ultimately guarantees the convergence of the iQCC procedure.²⁹ The whole $\{\hat{X}_m\}$, however, may not contain enough operators to

find n primary and $(n - 1)$ secondary vectors to construct the maximal anti-commutative set. In such a situation we do *not* construct complementary operators as they will have zero gradients and their energy impact is unclear. On the other hand, in the case of extremely large $\{\hat{X}_m\}$ it may be necessary to drop some operators from consideration, and those with the smallest gradients are the first candidates. Operators from $\{\hat{X}_m\}$ may have vanishing gradients because of special symmetry of the qubit reference vector $|0\rangle$ —for example, when $|0\rangle$ is an eigenvector of $\hat{I}_k(\mathbf{z})$ for some $k > 0$ with 0 as an eigenvalue^b. In what follows we do not drop operators from $\{\hat{X}_m\}$ with vanishing gradients to simplify the discussion.

2.2.8 Algorithm summary

Algorithm 1: A set of anti-commuting Pauli words from a set of X words

Input : A sequence of X words $\{\hat{X}_m\}$

Output: $\{\hat{X}_{m_l}\} \subset \{\hat{X}_m\}$ and $\{\hat{Z}_{m_l}\}$ such that $\hat{T}_{m_l} = \hat{X}_{m_l} \odot \hat{Z}_{m_l}$ and $[\hat{T}_l, \hat{T}_{l'}]_+ = 2\delta_{ll'}$

```

1 foreach  $\hat{X}_k \in \{\hat{X}_m\}$  do // form a M matrix
2   |  $\mathbf{M}[:, k] = \text{BinaryRepresentation}(\hat{X}_k)$ 
3   |  $k \leftarrow k + 1$ 
4 end
5  $\mathbf{M}_{\text{rref}}, \mathbf{R} \leftarrow \text{rref}(\mathbf{M})$  // Gauss--Jordan elimination
6 Identify primary and secondary columns of  $\mathbf{M}_{\text{rref}}$ 
7  $\{\hat{X}_{m_l}\}$ : select from  $\{\hat{X}_m\}$  operators that correspond to primary and secondary
   column indices
8 Construct primary and secondary binary vectors  $\{Z_k\}$  for every primary and
   secondary column in  $\mathbf{M}_{\text{rref}}$  using Table 2.
9 Transform  $\{Z_k\}$  from the standard to the original basis:  $Z_k \leftarrow \mathbf{R}^T Z_k$ 
10  $\{\hat{Z}_{m_l}\}$ : Convert binary vectors  $\{Z_k\}$  back to the operator form

```

2.3 Perturbative correction for QCC-ILCAP

The size of any anti-commuting system $\sim n$ is fundamentally limited by the qubit dimensionality of a system. Since the number of groups of operators with non-zero gradients in the

^bThe corresponding gradient value $\omega_k = 0$ according to Eq. (21)

qubit image of a fermionic Hamiltonian (14) is $O(n^4)$, the bulk of energy lowering due to correlation will *not* be captured by the QCC-ILCAP Ansatz in a single iteration. Though a fully iterative procedure is possible, a single application of QCC-ILCAP as a pre- and especially post-processing technique calls for a completeness correction. As such, we propose a Brillouin–Wigner perturbation theory at the second order motivated by theoretical simplicity and computational efficiency of this approach. Namely, the unitary QCC-ILCAP Ansatz is equivalent to a linear parametrization of a variational wave function, as follows from Eq. (9). Thus, the energy functional (22) is a quadratic form

$$E_{\text{ILCAP}}(\mathbf{C}) = \mathbf{C}^\dagger \mathbf{H} \mathbf{C}, \quad (34)$$

where \mathbf{H} is an $(M + 1) \times (M + 1)$ matrix with elements

$$H_{k'k} = \begin{cases} \langle 0 | \hat{H} | 0 \rangle, & k' = k = 0, \\ i \langle 0 | \hat{T}_{k'} \hat{H} | 0 \rangle, & 1 \leq k' \leq M, k = 0, \\ -i \langle 0 | \hat{H} \hat{T}_k | 0 \rangle, & 1 \leq k \leq M, k' = 0, \\ \langle 0 | \hat{T}_{k'} \hat{H} \hat{T}_k | 0 \rangle, & 1 \leq k', k \leq M, \end{cases} \quad (35)$$

$\hat{T}_{k'}$ and \hat{T}_k are operators from ILCAP and components of a vector \mathbf{C} are related to cluster amplitudes $(t, \boldsymbol{\alpha})$ as

$$C_0 = \cos\left(\frac{t}{2}\right), \quad (36)$$

$$C_i = \alpha_i \sin\left(\frac{t}{2}\right), \quad 1 \leq i \leq M. \quad (37)$$

Choosing anti-commuting generators \hat{T}_k with the odd number of \hat{y} ensures the matrix elements (35) are all real. Extrema of the functional (34) are eigenvectors of \mathbf{H} that can be chosen orthonormal; the one which corresponds to the lowest eigenvalue is used to recover amplitudes by Eqs. (36) and (37).

The relation of the energy minimization with the QCC-ILCAP Ansatz with the eigenvalue problem $\mathbf{H}\mathbf{C} = E\mathbf{C}$ provides a unique opportunity to apply a Brillouin–Wigner perturbation theory via the Löwdin partitioning.⁴³ Consider a rectangular matrix \mathbf{b} with elements

$$b_{km} = \begin{cases} \langle 0 | \hat{H} \hat{X}_m | 0 \rangle, & k = 0, \\ i \langle 0 | \hat{T}_k \hat{H} \hat{X}_m | 0 \rangle, & 1 \leq k \leq M, \end{cases} \quad (38)$$

and a diagonal matrix \mathbf{D} with elements $\langle 0 | \hat{X}_m \hat{H} \hat{X}_m | 0 \rangle$, where \hat{X}_m are operators from the Ising decomposition of \hat{H} that were *not* used to construct ILCAP. Then the Brillouin–Wigner ground-state energy estimate is the lowest eigenvalue of an energy-dependent matrix

$$\mathbf{H}^{\text{eff}}(E) = \mathbf{H} - \mathbf{b}(\mathbf{D} - E)^{-1}\mathbf{b}^\dagger. \quad (39)$$

Due to the energy dependence of \mathbf{H}^{eff} , iterations are necessary to obtain the ground-state energy estimate, $E_{\text{ILCAP+BW}}$. However, computational time and memory storage requirements for both \mathbf{b} and \mathbf{D} matrices are linearly proportional to the size of a Hamiltonian (more accurately, $\{\hat{X}_m\}$ set).

To perform the completeness correction one can alternatively apply the Epstein–Nesbet perturbation theory³⁰ after the dressing of the current Hamiltonian (see Sec. 2.1) with the optimized QCC-ILCAP transformation. While this approach is not viable as a post-processing technique, it cross-validates applicability of the perturbation theory.

3 Results and discussion

3.1 General setup

To illustrate our developments we compute potential energy curves for the symmetric stretch of an H₂O molecule and dissociation of N₂. Both processes describe a graduate transition from weak to strong correlation; a robust method must not break down upon this transition. Two

considered models differ in their qubit dimensionality: the first one is a mid-scale 36-qubit problem while the second is a large-scale 56 qubit one.

For each molecule we consider the following schemes:

1. **QCC-ILCAP as a pre-processing technique.** We optimize the QCC-ILCAP Ansatz (9) to find an approximate ground state $|\Psi\rangle_{\text{ILCAP}} = \hat{U}_{\text{ILCAP}}(t_{\text{opt}}, \boldsymbol{\alpha}_{\text{opt}}) |0\rangle$, the corresponding ground-state energy estimate $E_{\text{ILCAP}} = \langle \Psi_{\text{ILCAP}} | \hat{H} | \Psi_{\text{ILCAP}} \rangle$, and its Brillouin–Wigner-corrected counterpart, $E_{\text{ILCAP+BW}}$, computed as described in Sec. 2.3. Here \hat{H} is a fermionic Hamiltonian (12) converted to the qubit representation. At this point, the QCC-ILCAP approach can be considered as a quantum-inspired method for adding the electron correlation to a mean-field description (encoded as $|0\rangle$) of a molecular ground state. Next, aiming at the use of the QCC-ILCAP optimized unitary to facilitate electronic structure calculations on NISQ devices, we define the ILCAP-dressed Hamiltonian, $\hat{H}_{\text{ILCAP}} = \hat{U}_{\text{ILCAP}}^\dagger(t_{\text{opt}}, \boldsymbol{\alpha}_{\text{opt}}) \hat{H} \hat{U}_{\text{ILCAP}}(t_{\text{opt}}, \boldsymbol{\alpha}_{\text{opt}})$. To simulate the further use of \hat{H}_{ILCAP} on a quantum computer, we evaluate the Epstein–Nesbet perturbation theory correction (denoted as $E_{\text{ILCAP+EN}}$) to the ground-state energy estimate $\langle 0 | \hat{H}_{\text{ILCAP}} | 0 \rangle \equiv E_{\text{ILCAP}}$ as described in Ref. 30.
2. **QCC-ILCAP as a post-processing technique.** We perform several rounds of the iQCC procedure as described in Sec. 2.1 and take the last dressed Hamiltonian, $\hat{H}^{(i+1)}$ ($i \geq 1$) as the starting one for the application of the QCC-ILCAP Ansatz. After optimization of amplitudes ($t, \boldsymbol{\alpha}$) we consider the final energy, $E_{\text{QCC}(i)+\text{ILCAP}}$ as well as its Brillouin–Wigner-corrected partner, $E_{\text{QCC}(i)+\text{ILCAP+BW}}$ as new ground-state estimates and compare them to the “bare” iQCC energies and their Epstein–Nesbet-corrected counterparts denoted as $E_{\text{QCC}(i)}$ and $E_{\text{QCC}(i)+\text{EN}}$, respectively.

For both molecules we prepared a set of restricted Hartree–Fock (RHF) MOs which were subsequently used to compute one- and two-electron integrals in the active space. These calculations were carried out using a modified version of GAMESS,^{44,45} from Sep 30, 2019

(R2).

The common setup for the iQCC method is as follows. Generators were ranked according to the “optimal amplitude” defined by Eq. 33 of Ref. 30 as it works slightly better than the gradient ranking in the case of strong correlation (highly stretched geometries). To stay on a singlet solution along the whole potential curve we added a penalty operator \hat{W} to the initial Hamiltonians at every nuclear configuration,

$$\hat{H} \rightarrow \hat{H} + \frac{\mu}{2}\hat{W}, \tag{40}$$

$$\hat{W} = \hat{S}^2 - (2s + 1)\hat{S}_z + s^2, \tag{41}$$

where \hat{S}^2 and \hat{S}_z are the qubit images of the total spin squared operator and its z projection, respectively, $s = 0$ is a spin quantum number for a singlet state, and μ is a penalty parameter.

3.2 H₂O simulations

The RHF MOs were expanded in 6-31G(d) atomic basis set⁴⁶ with a six-component (Cartesian) d polarisation function assuming C_{2v} symmetry at selected O–H distances and fixed $\angle\text{HOH} = 107.60^\circ$. The lowest-energy MO that correlates with an $1s$ atomic orbital of oxygen atom was frozen while the remaining 18 orbitals were considered as active. This leads to a 36-qubit Hamiltonian (14) with 41 915 qubit terms; all terms with coefficients smaller than 10^{-8} in magnitude were discarded. The spin-penalty strength parameter μ [see Eq. (40)] was set to 0.025; the number of terms in the penalized operator is 42 527. The qubit reference vector (15) represents an eight-electron closed-shell singlet state ($n_e = 8$).

QCC-ILCAP as a pre-processing technique. For every value of $d(\text{O–H})$ we report three ground-state energy estimates^c, E_{ILCAP} , $E_{\text{ILCAP+BW}}$, and $E_{\text{ILCAP+EN}}$ computed as described in Sec. 3.1. We compare them against CASCI values (denoted as $E_{\text{FCI(m1s)}}$)

^cThe nuclear-nuclear repulsion energy V_{nn} is added for the total electronic energy at every nuclear configuration.

computed by the Davidson diagonalization of the fermionic Hamiltonian in the determinant basis in GAMESS. In C_{2v} symmetry this basis contains 2 342 224 determinants with $s_z = 0$. The resulting potential energy curves are shown in Fig. 1.

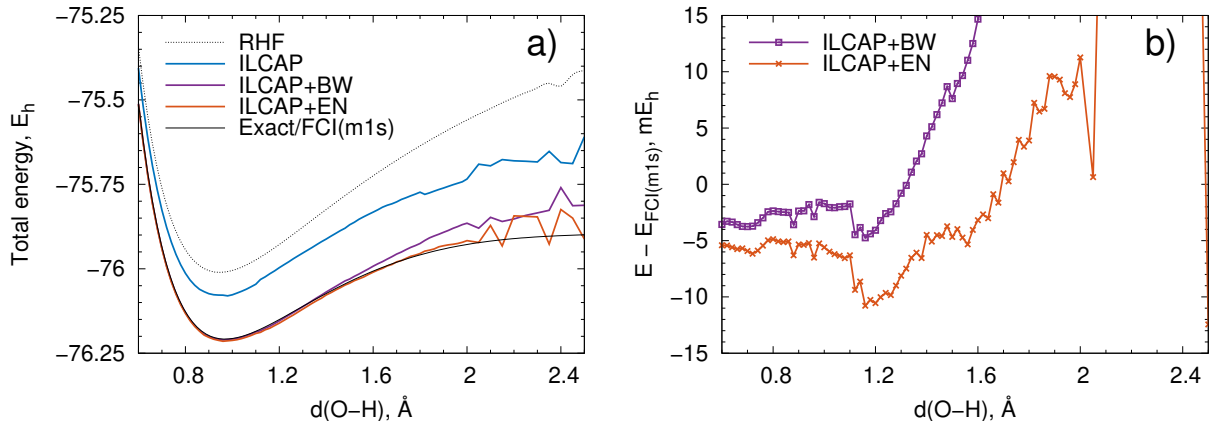


Figure 1: a) Potential energy curves for symmetric O–H stretching of H_2O molecule. b) Deviations of the energy (in mE_h) from the exact-diagonalization result denoted as FCI(m1s)

As follows from Fig. 1a, QCC-ILCAP provides a reasonably smooth potential energy curve for $d(\text{O-H}) \lesssim 1.8 \text{ \AA}$, while for ILCAP+BW and ILCAP+EN schemes this range extends to $d(\text{O-H}) \approx 2.0 \text{ \AA}$. However, closer inspection of seemingly good curves for those two schemes in a range $0.6\text{--}2.0 \text{ \AA}$ (see Fig. 1b) reveals a saw-tooth pattern with oscillations of a few millihartree in magnitude superimposed on gradually increasing deviation from the exact result. Such non-smooth potential energy curves for the QCC method were already reported³² and were attributed to re-ordering of generators employed in the construction of the QCC Ansatz. Here we construct a QCC-ILCAP of the maximal possible size using *all* generators with a priori non-zero gradients; despite this, “kinks” still have an appreciable magnitude greater than the so-called “chemical accuracy” of $\sim 1 mE_h$. Kinks of smaller amplitude are likely due to re-ordering of generators with non-maximal importance measure. However, the first large kink near $d(\text{O-H}) \approx 2.1 \text{ \AA}$ is due to the change of the leading (top-ranked, first) generator. The top-ranked generator (out of 47 included in ILCAP) at $d(\text{O-H}) = 2.05 \text{ \AA}$ has $\hat{x}_6\hat{x}_7\hat{x}_{10}\hat{x}_{11}$ parental X word, while at $d(\text{O-H}) = 2.1 \text{ \AA}$ the top-ranked generator (out of 43 in the whole ILCAP) stems from the $\hat{x}_6\hat{x}_7\hat{x}_8\hat{x}_9$ word which again becomes $\hat{x}_6\hat{x}_7\hat{x}_{10}\hat{x}_{11}$

at $d(\text{O-H}) = 2.15 \text{ \AA}$ with 50 operators in the entire ILCAP. These substantial changes in composition of ILCAP are reflected in large variations of E_{ILCAP} , $E_{\text{ILCAP+BW}}$, and $E_{\text{ILCAP+EN}}$ in the small range 2.05–2.15 \AA of O–H distances.

Overall, the QCC-ILCAP method captures less than a half of the total correlation energy and requires the perturbation correction to account for the rest. The Brillouin–Wigner approach indeed brings the total energy to be a few millihartree away from the exact value, but only if the electron correlation is not too strong. The ILCAP+EN scheme performs slightly better but still suffers from large variations near the dissociation limit.

QCC-ILCAP as a post-processing technique. We have performed four ($i = 4$) iQCC iterations with $L = 12$ generators in Eq. (2) and constructed the ILCAP Ansatz based on the Ising decomposition of $\hat{H}^{(5)}$ Hamiltonian [see Eq. (23)]. We report four energy estimates, $E_{\text{QCC}(4)} = \langle 0 | \hat{H}^{(5)} | 0 \rangle$, $E_{\text{QCC}(4)+\text{EN}}$, $E_{\text{QCC}(4)+\text{ILCAP}}$, and $E_{\text{QCC}(4)+\text{ILCAP+BW}}$, which are shown in Fig. 2. Figure 2a demonstrates that preliminary iQCC iterations account for 40–60 % of

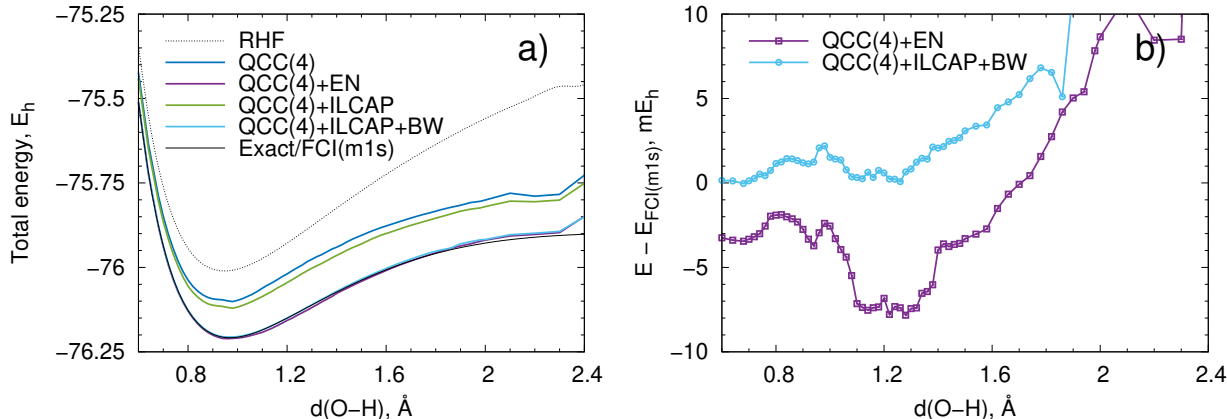


Figure 2: Same as for Fig. 1.

the correlation energy while the subsequent ILCAP treatment adds relatively small amount of the remaining correlation energy. Both perturbation corrections, the Epstein-Nesbet one on top of QCC(4) and Brillouin–Wigner on top of the QCC(4)+ILCAP wave function provide comparable accuracy. The QCC(4)+ILCAP+BW scheme appears to be superior to the QCC(4)+EN counterpart giving a smoother curve with a deviation of 0–5 mE_h in the range

of $d(\text{O}-\text{H})$ 0.6–1.8 Å. Comparison of Figs. 1 and 2 shows that the preceding iQCC iterations not only mitigate the problem of non-smooth potential energy curves but also help ILCAP and especially ILCAP+BW schemes to provide more accurate energies in a wider range of O–H distances.

3.3 N₂ simulations

The RHF orbitals were expanded in Dunning’s cc-pVDZ atomic basis set⁴⁷ assuming D_{2h} symmetry of a molecule. All 28 orbitals and 14 electrons were taken as active, so the second-quantized Hamiltonians (12) represented a FCI problem; the corresponding 56-qubit Hamiltonians contained 107 881 Pauli terms at every value of $d(\text{N}-\text{N})$. Terms smaller than 10^{-7} were dropped from the initial and dressed Hamiltonians. The spin-penalty strength μ [see Eqs. (40) and (41)] was set to 0.125, the penalized Hamiltonian had 109 393 terms.

The FCI energies were taken from Ref. 48 as the conventional FCI calculations are not possible even with supercomputer resources. The FCI energy estimates are believed to be accurate to $1 \times 10^{-6} E_h$.

QCC-ILCAP as a pre-processing technique. E_{ILCAP} , $E_{\text{ILCAP+BW}}$, and $E_{\text{ILCAP+EN}}$ along with FCI and RHF curves are plotted in Fig. 3. Compared with Fig. 1 kinks on ILCAP,

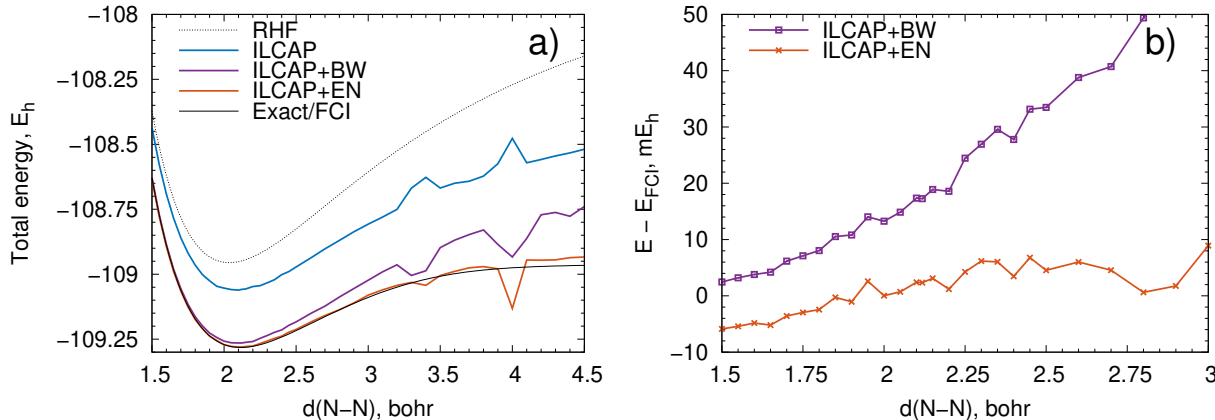


Figure 3: Same as for Fig. 1 but for the N₂ molecule stretching.

ILCAP+BW and ILCAP+EN curves appear earlier, already at $\sim 1.5R_e$, and have larger

amplitudes. This is expected as correlation is stronger for a triple-bond breaking process. Just like in the case of H_2O the most noticeable kinks are related to changes in the leading (top-ranked) generator used to construct the QCC-ILCAP Ansatz: at $d(\text{N}-\text{N}) = 3.2 a_0$ the top-ranked generator stems from the $\hat{x}_{10}\hat{x}_{11}\hat{x}_{14}\hat{x}_{15}$ X word, which changes into $\hat{x}_{10}\hat{x}_{13}\hat{x}_{15}\hat{x}_{16}$ at $d(\text{N}-\text{N}) = 3.3 a_0$, then to $\hat{x}_{12}\hat{x}_{13}\hat{x}_{14}\hat{x}_{15}$ at $d(\text{N}-\text{N}) = 3.4 a_0$ and finally returns back to $\hat{x}_{10}\hat{x}_{11}\hat{x}_{14}\hat{x}_{15}$ at $d(\text{N}-\text{N}) = 3.5 a_0$.

Quantitatively, the deviations from the FCI values are 2–5 times larger than those in Fig. 1; however, they are accumulated more uniformly. Somewhat surprisingly, the ILCAP+EN scheme based on the ILCAP-dressed Hamiltonian is closer to the FCI reference than any other schemes, staying within -6 to $6 mE_h$ in the range of N–N distances 1.5 – $3.0 a_0$. Perhaps, this is because the second-order perturbation theory based on the dressed Hamiltonian contains higher-order contributions in terms of the original fermionic Hamiltonian which are more important for triple-bond breaking process than for the simultaneous breaking of only two bonds in H_2O .

QCC-ILCAP as a post-processing technique. We performed $i = 4$ iQCC iterations with $L = 14$ generators, and the ILCAP Ansatz was constructed using the $\hat{H}^{(5)}$ dressed Hamiltonian. The number of terms in the Ising decomposition (19) of $\hat{H}^{(5)}$ varied with $d(\text{N}-\text{N})$ peaking at 45×10^6 .

Potential energy curves for four QCC-based schemes, $E_{\text{QCC}(4)} = \langle 0 | \hat{H}^{(5)} | 0 \rangle$, $E_{\text{QCC}(4)+\text{EN}}$, $E_{\text{QCC}(4)+\text{ILCAP}}$, and $E_{\text{QCC}(4)+\text{ILCAP}+\text{BW}}$ are displayed in Fig. 4. Preceding iQCC iterations solved the problem of large kinks on the potential energy curves for all considered schemes. As evident from Fig. 4b, the remaining variations are of the order of $1 mE_h$ or less, with increasing deviation from FCI upon increasing of the N–N distance. The overall quality of the two best variants, $E_{\text{QCC}(4)+\text{ILCAP}+\text{BW}}$ or $E_{\text{QCC}(4)+\text{EN}}$, is very close; the former is shifted upwards compared to the FCI reference. In order to assess the quality of *relative* energies, we fitted the total energies in the range of N–N distances 1.5 – $3.0 a_0$ to the Morse potential

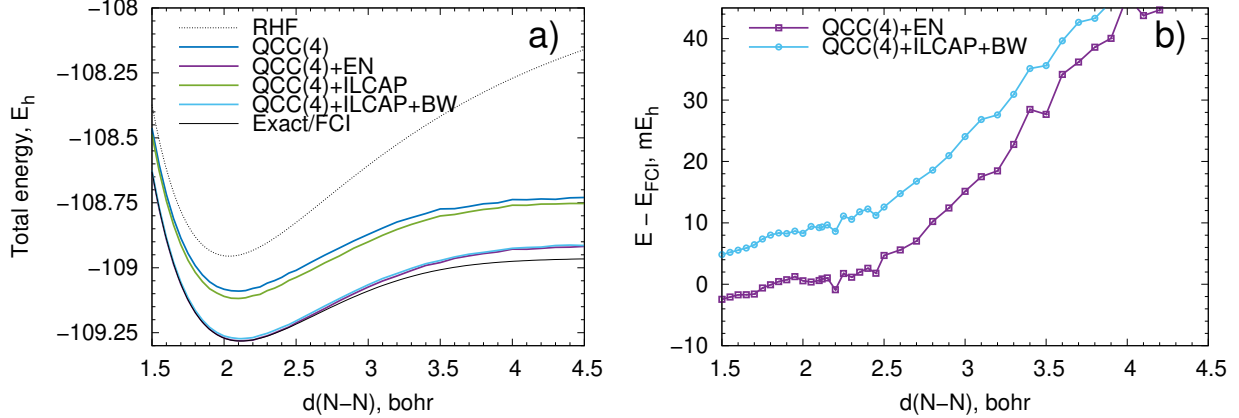


Figure 4: Same as for Fig. 1 but for the N_2 molecule stretching.

curve,

$$E(r) = D_e (1 - e^{-a(r-r_e)})^2 + E_{\min}, \quad (42)$$

where D_e is the dissociation energy, r_e is the position of the minimum, $E_{\min} = E(r_e)$, and a is a parameter related to the force constant. From this fit we computed the spectroscopic properties, namely, the harmonic frequency ω_e and the first anharmonicity constant $\omega_e x_e$ as

$$\omega_e = a \sqrt{\frac{2D_e}{\mu}} \quad (43)$$

$$\omega_e x_e = \frac{\omega_e^2}{4D_e}, \quad (44)$$

where μ is the reduced mass of a $^{14}N_2$ species, $\mu = m_N/2 = 7.00155$ u. All quantities are collected in Table 3. We have to mention that the Morse potential does *not* approximate well

Table 3: Spectroscopic constants of the N_2 from the Morse fitting, Eq. (42).

Method	E_{\min}	D_e	r_e, a_0	a, a_0^{-1}	RMS of residuals	ω_e	$\omega_e x_e$
	E_h					cm^{-1}	
QCC(4)+EN	-109.2819	0.4434	2.112	1.295	9.68×10^{-4}	2369	14.4
QCC(4)+ILCAP+BW	-109.2732	0.4402	2.110	1.301	7.65×10^{-4}	2371	14.6
FCI	-109.2821	0.4022	2.115	1.335	1.94×10^{-4}	2326	15.3

the realistic molecular potential especially for highly stretched configurations,⁴⁹ so the values of D_e from the fit overestimate the true dissociation energy of N_2 ($D_e = 228.42$ kcal mol $^{-1}$ =

0.3640 E_h ⁵⁰). However, near-equilibrium properties, such as r_e itself, ω_e , and $\omega_e x_e$ are accurate if fit is performed not far from the minimum. Data in Table 3 confirm that r_e , ω_e , and $\omega_e x_e$ for QCC(4)+ILCAP+BW and QCC(4)+EN curves are very close. The root mean square (RMS) of residuals for the former, however, is smaller than for the latter which implies the QCC(4)+ILCAP+BW curve is smoother.

3.4 Order-dependence of iQCC-ILCAP energies

The unitary (2), which is the final form for many VQE-based methods, is order-dependent due to non-commutativity of some of generators \hat{T}_k . This order-dependence has important ramifications for state optimizations: it was demonstrated that *some* orderings may not approximate selected FCI states with arbitrary accuracy^{51,52} or may display large, of the order of hundreds kcal mol⁻¹, energy errors compared to alternative orderings.⁵³

Despite the “ultimate” anti-commutativity demanded by Eq. (11), the QCC-ILCAP Ansatz is order-independent, which immediately follows from its equivalence to a linear parametrization (9). However, some order-dependence is brought into by the construction algorithm. On the one hand, the reduced row-echelon form \mathbf{M}_{rref} (see Sec. 2.2.4) is unique for a given matrix \mathbf{M} . On the other, different ordering of columns essentially implies that one has multiple matrices \mathbf{M} , each of those leads to different anti-commutative set of Paulis. We fix the order of columns by sorting them in accordance with descending “importance measure”, which is a smooth function of Hamiltonian’s coefficients; see Sec. 2.2.7. Unfortunately, some drastic changes in composition of the anti-commutative set are still possible when several generators acquire numerically identical measure values. These degeneracies may be symmetry-related, if coefficients of the Hamiltonian become equal by symmetry, or accidental. The symmetry-related degeneracies may be fixed by introducing additional, for example lexicographical, ordering of generators. The accidental degeneracies are more problematic. In fact, all large kinks that are visible in Figs. 1 and 3 are due to accidental degeneracies. The odds for accidental degeneracies to occur increase with increasing the density of states at

the particular nuclear configuration and a degree of their mixing – that is why kinks show up with larger probabilities when chemical bonds are “half-broken”. Unfortunately, it is not clear how this issue could be fixed, which warrants future studies.

4 Conclusions

We have presented a novel algorithm for efficient construction of fully-anticommutative sets of Pauli generators (3) that are tagged by additional properties, such as energy gradients. We applied the Gaussian elimination procedure over the GF(2) field to matrices that represent Pauli X words to determine the primary and secondary vectors (operators) in a standard basis, from which the anti-commutative system is constructed by means of a slightly modified Jordan–Wigner transformation. Returning from the standard to the original system of Paulis is encoded by the matrices \mathbf{R}^{-1} and \mathbf{R}^T (see Sec. 2.2.4) for Pauli X and Z words, respectively, and only the latter must be explicitly computed. The algorithm complexity is linear in the size of the input set and quadratic in the number of qubits, which allows one to apply it to systems with hundreds of qubits and Hamiltonians containing tens of millions terms in their Ising decomposition (19).

To demonstrate the scalability of our algorithm we have applied the QCC-ILCAP treatment to the symmetric stretch of the H₂O molecule and dissociation of N₂. Both problems are considered in reasonably large basis sets, 6-31G(d) and cc-pVDZ, respectively, which leads to 36- and 56-qubit initial Hamiltonians containing up to 10⁵ terms.

The QCC-ILCAP Ansatz was applied before (termed as pre-processing) and after (post-processing) ordinary iQCC iterations. As a pre-processing technique, the QCC-ILCAP Ansatz has a limited ability to recover the correlation energy; to account for the remaining piece we proposed the use of the Brillouin–Wigner perturbation theory. The QCC-ILCAP+BW scheme can be considered as a state-specific (ground-state) multiconfigurational perturbation theory formulated in terms of qubit, rather than fermionic, generators. Even with the

perturbative correction, the QCC-ILCAP treatment encounters difficulties in the case of strong correlation which manifest themselves in non-continuous potential energy curves. Overall, the QCC-ILCAP and QCC-ILCAP+BW schemes are not as robust as more traditional multiconfigurational theories, and in the present form do not allow for treatment of excited states. However, the computational complexity is low and is comparable to that of single-reference [e.g. the second-order Møller–Plesset perturbation theory (MP2)] perturbation theories.

The QCC-ILCAP treatment is most promising as a post-processing technique. The difficulties that the QCC-ILCAP treatment experiences with strongly correlated systems are less relevant since for dressed Hamiltonians the strength of correlation is systematically diminished. A single application of the QCC-ILCAP Ansatz amounts to 2–4 regular iQCC iterations for the given qubit dimensionality (40–60 qubits). For larger systems this “efficiency ratio” is likely to increase because the regular QCC Ansatz is difficult to optimize (on a classical computer) for more than $L \sim 20$ amplitudes due to exponential complexity, whereas the ILCAP construction and subsequent QCC-ILCAP optimizations are easily done for hundreds of them. Because of the variational nature, the QCC-ILCAP energies may be taken as extrapolation to the iQCC energies when additional iQCC iterations are not possible due to the excessive size of the dressed Hamiltonian. The QCC(n)+ILCAP+BW scheme, on the other hand, does not significantly improve upon the QCC(n)+EN counterpart, but provides smoother potential energy curves. The energy discrepancy between these two schemes can be used to gauge the reliability of energy estimates. The QCC-ILCAP treatment has already been used for this purpose in large-scale simulations of organic light-emitting diode (OLED) materials.³¹

Acknowledgement

The IGR and SNG thanks Prof. Artur F. Izmaylov and Robert A. Lang for many fruitful

discussions.

References

- (1) Cao, Y.; Romero, J.; Olson, J. P.; Degroote, M.; Johnson, P. D.; Kieferová, M.; Kivlichan, I. D.; Menke, T.; Peropadre, B.; Sawaya, N. P. D.; Sim, S.; Veis, L.; Aspuru-Guzik, A. Quantum Chemistry in the Age of Quantum Computing. *Chem. Rev.* **2019**, *119*, 10856–10915.
- (2) Bauer, B.; Bravyi, S.; Motta, M.; Kin-Lic Chan, G. Quantum Algorithms for Quantum Chemistry and Quantum Materials Science. *Chem. Rev.* **2020**, *120*, 12685–12717.
- (3) McArdle, S.; Endo, S.; Aspuru-Guzik, A.; Benjamin, S. C.; Yuan, X. Quantum computational chemistry. *Rev. Mod. Phys.* **2020**, *92*, 015003.
- (4) Motta, M.; Rice, J. E. Emerging quantum computing algorithms for quantum chemistry. *Wiley Interdiscip. Rev. Comput. Mol. Sci.* **2022**, *12*, e1580.
- (5) Tilly, J.; Chen, H.; Cao, S.; Picozzi, D.; Setia, K.; Li, Y.; Grant, E.; Wossnig, L.; Rungger, I.; Booth, G. H.; Tennyson, J. The Variational Quantum Eigensolver: a review of methods and best practices. *arXiv e-prints* **2021**, 2111.05176v2.
- (6) Preskill, J. Quantum Computing in the NISQ era and beyond. *Quantum* **2018**, *2*, 79.
- (7) Peruzzo, A.; McClean, J.; Shadbolt, P.; Yung, M.-H.; Zhou, X.-Q.; Love, P. J.; Aspuru-Guzik, A.; O’Brien, J. L. A variational eigenvalue solver on a photonic quantum processor. *Nat. Commun.* **2014**, *5*, 4213.
- (8) Poulin, D.; Kitaev, A.; Steiger, D. S.; Hastings, M. B.; Troyer, M. Quantum Algorithm for Spectral Measurement with a Lower Gate Count. *Phys. Rev. Lett.* **2018**, *121*, 010501.

- (9) Huggins, W. J.; McClean, J.; Rubin, N.; Jiang, Z.; Wiebe, N.; Whaley, K. B.; Babbush, R. Efficient and Noise Resilient Measurements for Quantum Chemistry on Near-Term Quantum Computers. *arXiv e-prints* **2019**, 1907.13117.
- (10) Crawford, O.; van Straaten, B.; Wang, D.; Parks, T.; Campbell, E.; Brierley, S. Efficient quantum measurement of Pauli operators. *arXiv e-prints* **2019**, 1908.06942.
- (11) Verteletskyi, V.; Yen, T.-C.; Izmaylov, A. F. Measurement optimization in the variational quantum eigensolver using a minimum clique cover. *J. Chem. Phys.* **2020**, *152*, 124114.
- (12) Izmaylov, A. F.; Yen, T.-C.; Ryabinkin, I. G. Revising the measurement process in the variational quantum eigensolver: is it possible to reduce the number of separately measured operators? *Chem. Sci.* **2019**, *10*, 3746–3755.
- (13) Yen, T.-C.; Verteletskyi, V.; Izmaylov, A. F. Measuring All Compatible Operators in One Series of Single-Qubit Measurements Using Unitary Transformations. *J. Chem. Theory Comput.* **2020**, *16*, 2400–2409.
- (14) Schuld, M.; Bergholm, V.; Gogolin, C.; Izaac, J.; Killoran, N. Evaluating analytic gradients on quantum hardware. *Phys. Rev. A* **2019**, *99*, 032331.
- (15) Izmaylov, A. F.; Lang, R. A.; Yen, T.-C. Analytic gradients in variational quantum algorithms: Algebraic extensions of the parameter-shift rule to general unitary transformations. *Phys. Rev. A* **2021**, *104*, 062443.
- (16) Piskor, T.; Reiner, J.-M.; Zanker, S.; Vogt, N.; Marthaler, M.; Wilhelm, F. K.; Eich, F. G. Using gradient-based algorithms to determine ground-state energies on a quantum computer. *Phys. Rev. A* **2022**, *105*, 062415.
- (17) Kandala, A.; Mezzacapo, A.; Temme, K.; Takita, M.; Brink, M.; Chow, J. M.; Gambetta, J. M. Hardware-efficient variational quantum eigensolver for small molecules and quantum magnets. *Nature* **2017**, *549*, 242–246.

- (18) Nielsen, M.; Chuang, I. *Quantum Computation and Quantum Information: 10th Anniversary Edition*; Cambridge University Press, 2010.
- (19) Ref. 18, chap 10.5.1.
- (20) Ortiz, G.; Gubernatis, J. E.; Knill, E.; Laflamme, R. Quantum algorithms for fermionic simulations. *Phys. Rev. A* **2001**, *64*, 022319.
- (21) Wecker, D.; Hastings, M. B.; Troyer, M. Progress towards practical quantum variational algorithms. *Phys. Rev. A* **2015**, *92*, 042303.
- (22) McClean, J. R.; Romero, J.; Babbush, R.; Aspuru-Guzik, A. The theory of variational hybrid quantum-classical algorithms. *New J. Phys.* **2016**, *18*, 023023.
- (23) O’Malley, P. J. J.; Babbush, R.; Kivlichan, I. D.; Romero, J.; McClean, J. R.; Barends, R.; Kelly, J.; Roushan, P.; Tranter, A.; Ding, N.; Campbell, B.; Chen, Y.; Chen, Z.; Chiaro, B.; Dunsworth, A.; Fowler, A. G.; Jeffrey, E.; Lucero, E.; Megrant, A.; Mutus, J. Y.; Neeley, M.; Neill, C.; Quintana, C.; Sank, D.; Vainsencher, A.; Wenner, J.; White, T. C.; Coveney, P. V.; Love, P. J.; Neven, H.; Aspuru-Guzik, A.; Martinis, J. M. Scalable Quantum Simulation of Molecular Energies. *Phys. Rev. X* **2016**, *6*, 031007.
- (24) Romero, J.; Babbush, R.; McClean, J. R.; Hempel, C.; Love, P. J.; Aspuru-Guzik, A. Strategies for quantum computing molecular energies using the unitary coupled cluster ansatz. *Quantum Sci. Technol.* **2018**, *4*, 014008.
- (25) Ryabinkin, I. G.; Yen, T.-C.; Genin, S. N.; Izmaylov, A. F. Qubit Coupled Cluster Method: A Systematic Approach to Quantum Chemistry on a Quantum Computer. *J. Chem. Theory Comput.* **2018**, *14*, 6317–6326.
- (26) Grimsley, H. R.; Economou, S. E.; Barnes, E.; Mayhall, N. J. An adaptive variational algorithm for exact molecular simulations on a quantum computer. *Nat. Commun.* **2019**, *10*, 3007.

- (27) Lee, J.; Huggins, W. J.; Head-Gordon, M.; Whaley, K. B. Generalized Unitary Coupled Cluster Wave functions for Quantum Computation. *J. Chem. Theory Comput.* **2019**, *15*, 311–324.
- (28) Nam, Y.; Chen, J.-S.; Picienti, N. C.; Wright, K.; Delaney, C.; Maslov, D.; Brown, K. R.; Allen, S.; Amini, J. M.; Apisdorf, J.; Beck, K. M.; Blinov, A.; Chaplin, V.; Chmielewski, M.; Collins, C.; Debnath, S.; Hudek, K. M.; Ducore, A. M.; Keesan, M.; Kreikemeier, S. M.; Mizrahi, J.; Solomon, P.; Williams, M.; Wong-Campos, J. D.; Moehring, D.; Monroe, C.; Kim, J. Ground-state energy estimation of the water molecule on a trapped-ion quantum computer. *npj Quantum Inf.* **2020**, *6*, 33.
- (29) Ryabinkin, I. G.; Lang, R. A.; Genin, S. N.; Izmaylov, A. F. Iterative Qubit Coupled Cluster Approach with Efficient Screening of Generators. *J. Chem. Theory Comput.* **2020**, *16*, 1055–1063.
- (30) Ryabinkin, I. G.; Izmaylov, A. F.; Genin, S. N. A posteriori corrections to the iterative qubit coupled cluster method to minimize the use of quantum resources in large-scale calculations. *Quantum Sci. Technol.* **2021**, *6*, 024012.
- (31) Genin, S. N.; Ryabinkin, I. G.; Paisley, N. R.; Whelan, S. O.; Helander, M. G.; Hudson, Z. M. Estimating Phosphorescent Emission Energies in Ir(III) Complexes Using Large-Scale Quantum Computing Simulations. *Angew. Chem. Int. Ed.* **2022**, *61*, e202116175.
- (32) Lang, R. A.; Ryabinkin, I. G.; Izmaylov, A. F. Unitary Transformation of the Electronic Hamiltonian with an Exact Quadratic Truncation of the Baker-Campbell-Hausdorff Expansion. *J. Chem. Theory Comput.* **2021**, *17*, 66–78.
- (33) McClean, J. R.; Boixo, S.; Smelyanskiy, V. N.; Babbush, R.; Neven, H. Barren plateaus in quantum neural network training landscapes. *Nat. Commun.* **2018**, *9*, 4812.

- (34) Helgaker, T.; Jorgensen, P.; Olsen, J. *Molecular Electronic-structure Theory*; Wiley, 2000.
- (35) Abrams, D. S.; Lloyd, S. Simulation of Many-Body Fermi Systems on a Universal Quantum Computer. *Phys. Rev. Lett.* **1997**, *79*, 2586–2589.
- (36) Aspuru-Guzik, A.; Dutoi, A. D.; Love, P. J.; Head-Gordon, M. Simulated Quantum Computation of Molecular Energies. *Science* **2005**, *309*, 1704–1707.
- (37) Jordan, P.; Wigner, E. Über das Paulische Äquivalenzverbot. *Z. Phys.* **1928**, *47*, 631–651.
- (38) Bravyi, S.; Gambetta, J. M.; Mezzacapo, A.; Temme, K. Tapering off qubits to simulate fermionic Hamiltonians. *ArXiv e-prints* **2017**, 1701.08213.
- (39) Meyer, C. D. *Matrix analysis and applied linear algebra*; Siam, 2000; Vol. 71.
- (40) Ref. [39](#), p 48.
- (41) Ref. [18](#), chap 10.5.2.
- (42) Ref. [18](#), chap 10.5.2.
- (43) Löwdin, P.-O. Studies in perturbation theory: II. Generalization of the Brillouin-Wigner formalism III. Solution of the Schrödinger equation under a variation of a parameter. *J. Mol. Spectrosc.* **1964**, *13*, 326 – 337.
- (44) Schmidt, M. W.; Baldrige, K. K.; Boatz, J. A.; Elbert, S. T.; Gordon, M. S.; Jensen, J. H.; Koseki, S.; Matsunaga, N.; Nguyen, K. A.; Su, S. J.; Windus, T. L.; Dupuis, M.; Montgomery, J. General Atomic and Molecular Electronic Structure System. *J. Comput. Chem.* **1993**, *14*, 1347–1363.
- (45) Gordon, M. S.; Schmidt, M. W. In *Theory and Applications of Computational Chemistry. The first forty years*; Dykstra, C. E., Frenking, G., Kim, K. S., Scuseria, G. E., Eds.; Elsevier: Amsterdam, 2005; pp 1167–1189.

- (46) Hehre, W. J.; Ditchfield, R.; Pople, J. A. Self—Consistent Molecular Orbital Methods. XII. Further Extensions of Gaussian—Type Basis Sets for Use in Molecular Orbital Studies of Organic Molecules. *J. Chem. Phys.* **1972**, *56*, 2257–2261.
- (47) Dunning, T. H. Gaussian basis sets for use in correlated molecular calculations. I. The atoms boron through neon and hydrogen. *J. Chem. Phys.* **1989**, *90*, 1007–1023.
- (48) Wang, Z.; Li, Y.; Lu, J. Coordinate Descent Full Configuration Interaction. *J. Chem. Theory Comput.* **2019**, *15*, 3558–3569.
- (49) Murrell, J. N.; Sorbie, K. S. New analytic form for the potential energy curves of stable diatomic states. *J. Chem. Soc., Faraday Trans. 2* **1974**, *70*, 1552–1556.
- (50) Martin, J. M. L. Very accurate ab initio binding energies — a comparison between empirical corrections and extrapolation methods. *J. Mol. Struct. THEOCHEM* **1997**, *398-399*, 135–144, World Congress of Theoretically Oriented Chemists.
- (51) Evangelista, F. A.; Chan, G. K.-L.; Scuseria, G. E. Exact parameterization of fermionic wave functions via unitary coupled cluster theory. *J. Chem. Phys.* **2019**, *151*, 244112.
- (52) Izmaylov, A. F.; Díaz-Tinoco, M.; Lang, R. A. On the order problem in construction of unitary operators for the variational quantum eigensolver. *Phys. Chem. Chem. Phys.* **2020**, *22*, 12980–12986.
- (53) Grimsley, H. R.; Claudino, D.; Economou, S. E.; Barnes, E.; Mayhall, N. J. Is the Trotterized UCCSD Ansatz Chemically Well-Defined? *J. Chem. Theory Comput.* **2020**, *16*, 1–6.